

A new numerical model of coupled inland ice sheet, ice stream, and ice shelf flow and its application to the West Antarctic Ice Sheet

Christina L. Hulbe¹ and Douglas R. MacAyeal

Department of Geophysical Sciences, University of Chicago, Chicago, Illinois

Abstract. We have developed a dynamic/thermodynamic finite element numerical model that couples inland ice sheet, ice stream, and ice shelf dynamics. This new model stands apart from other whole ice sheet models in its explicit treatment of ice stream flow. Additionally, the model accounts for both horizontal and vertical advection and diffusion of temperature in the flowing ice. In present day simulations of the West Antarctic Ice Sheet (WAIS), modeled ice velocity agrees well with observed ice flow. In particular, the model reproduces the pattern of speed variation across ice streams although the continuous downstream speed up of ice flow cannot be reproduced without concurrent downstream variation in basal friction. Model thermodynamics, evaluated qualitatively by model prediction of the spatial distribution of basal melting and quantitatively by comparison with ice temperature measured in boreholes at several locations, are sound. In particular, the model reproduces the broad pattern of frozen-bed inter-ice stream ridges and melted-bed ice streams. Model initialization for long-time simulations is somewhat limited by computation time and by a thermodynamic feedback at sites of large viscous heating that can be a problem in heat balance only model initializations. Methods for averting those initialization problems are discussed. The new model can accommodate a variety of boundary conditions (such as various bed rheologies) and is well-suited to investigate the origin and evolution of WAIS ice streams within the context of the whole ice sheet system.

1. Introduction

Many types of numerical models have been used to study aspects of West Antarctic Ice Sheet (WAIS) flow. In general, the strategy has been either to maximize resolution and consider one aspect of ice flow (e.g., ice stream margin dynamics [Raymond, 1996]) or to minimize resolution and simulate the bulk properties of the entire ice sheet system [cf. Fastook and Prentice, 1994; Huybrechts, 1990; Payne, 1995]. Both approaches to WAIS modeling have advanced knowledge of ice sheet behavior, but both are limited, in the scope of their predictive capability or in their ability to incorporate the unique attributes of an ice sheet with ice streams. Thus we sought to design a model which incorporates both modeling strategies.

The new numerical model accounts for many recent insights into the behavior of coupled inland ice sheet,

ice stream, and ice shelf systems. The version of the model described and tested here focuses on the physics of ice flow, but the model is designed to incorporate specialized routines for other physical processes that may affect ice sheet behavior (i.e., basal hydrology, till dynamics, sub ice shelf oceanography, or ice stream margin evolution). Such a model can be used as an experimental tool to study the interactions among flow regimes or to conduct sensitivity experiments regarding the effects of various boundary conditions on ice sheet flow. It can also be used as an interpretive tool in combination with observational data to test physical hypotheses about the origin of observed flow features. Finally, the model can be used as a prognostic tool to predict the flow of the ice sheet for a given future climate scenario or to retrodict flow based on constraints from the geologic record.

2. Numerical Model

2.1. Overview

The numerical model presented here is coupled dynamic/thermodynamic model that incorporates the varied dynamics of inland ice sheet, ice stream, and ice shelf flow regimes. It uses the finite element method to solve

¹Now at NASA Goddard Space Flight Center, Greenbelt, Maryland.

mass, stress, and heat continuity equations in a quasi-three-dimensional domain with appropriate boundary conditions, guided by logical evaluations made by model subroutines. The physical description of grounded inland ice and floating ice shelf ice is similar to the physics employed by other whole ice sheet models [cf. Budd *et al.*, 1987; Huybrechts, 1990]. A fundamental difference between this and other ice sheet models is in the physical description of ice stream flow. Also, because we use the finite element method, there are no special parameterizations at flow boundaries. With the condition that all ice arriving at an internal flow boundary must flow through it, ice flows smoothly from one regime to another (e.g., from the grounded ice sheet into the floating ice shelf). The variable resolution afforded by the selection of a triangular finite element mesh allows the model to fit any domain shape and to concentrate computational effort on features of particular interest.

2.2. Ice Sheet Physics

The mathematical expressions of ice sheet mass, stress, and heat balance are written in a Cartesian coordinate system, with x and y axes in the horizontal plane and the z axis positive upward. They have been derived elsewhere and are presented here in order to provide a complete representation of the dynamics and thermodynamics employed by the model.

2.3. Mass Balance

The change in ice sheet thickness over time is described by a mass continuity equation:

$$\frac{\partial h}{\partial t} = \dot{a} + \dot{b} - \nabla \cdot (\mathbf{u}h), \quad (1)$$

in which h represents ice thickness, t represents time, \dot{a} represents the ice accumulation rate at the upper surface, \dot{b} represents the ice accumulation rate at the lower surface, \mathbf{u} represents the horizontal ice velocity with boldface indicating a vector quantity. The surface accumulation rate is computed according to a climate parameterization. The basal accumulation rate, often a melt rate, is computed according to heat balance at the interface between the ice and the bed for the grounded ice sheet. Basal accumulation beneath the floating ice shelf is specified as a boundary condition. The quantity $(\mathbf{u}h)$ is a vector-valued mass flux, integrated over the ice thickness, in which \mathbf{u} derives from the solution of stress balance equations, with an appropriate flow law.

2.4. Stress Balance

The stresses which exert the most influence on ice flow differ in the inland, ice shelf, and ice stream regimes. In the inland ice sheet, ice flows over a rigid bed. Stress balance is between the pressure gradient due to surface slope, the "driving stress," and shear stresses between vertical layers, which are maximum near the bed, the "basal shear stress." The ice shelf flows over wa-

ter, a small-viscosity fluid compared to ice, so basal shear stress is near zero and stress balance is mainly between pressure gradients due to surface slope, which are largest near the seaward ice front, and a combination of horizontal normal stresses and lateral stresses due to flow past bay walls and ice rises. In the ice stream region, basal sediments have very small shear strength and basal water pressure is near the ice-overburden pressure with the consequence that shear stress is near zero and basal resistance to ice flow is small [Engelhardt and Kamb, 1997]. It is thus expected that ice stream stress balance is, in some sense, between that of inland ice and ice shelf ice. Here the driving stress in ice streams is balanced by lateral shearing at ice stream margins, by ice shelf back pressure, and by some form of resistance at the bed.

The stress balance equations for inland ice and for ice shelf ice are similar to those employed by numerous authors [cf. Huybrechts, 1990; MacAyeal, 1989]. In the inland ice sheet, expressions for horizontal strain rates are derived using the shallow-ice approximation [Hutter, 1983], Glen's flow law for ice [Paterson, 1981], and the assumption that ice is incompressible. Those equations, when integrated from the base of the ice sheet ($z = z_b$), using the boundary condition that horizontal velocity is zero at the base, yield equations for horizontal velocity:

$$u(z) = -2\rho g \frac{\partial z_s}{\partial x} \int_{z_b}^z EA (\rho g)^2 (\nabla z_s \cdot \nabla z_s) (z_s - z')^3 dz' \quad (2a)$$

$$v(z) = -2\rho g \frac{\partial z_s}{\partial y} \int_{z_b}^z EA (\rho g)^2 (\nabla z_s \cdot \nabla z_s) (z_s - z')^3 dz', \quad (2b)$$

where horizontal velocities u and v are in the x and y directions, respectively, z is the vertical coordinate, ρ represents ice density, g represents the acceleration due to gravity, and the top surface elevation z_s is the sum of the ice thickness and the bedrock elevation. E represents the traditional "enhancement factor" used to account for inadequacies in the flow law (always taken as 1 (one) here though in some ice sheet simulations, a value of 3 seems appropriate for Wisconsinan age ice). A represents the temperature-dependent rate factor for ice deformation by dislocation creep and the flow law exponent n is 3 [Hooke, 1981]. Where inland ice is at the local, pressure-dependent melt temperature at the bed, horizontal velocity (equations (2a) and (2b)) is augmented by basal sliding. The sliding parameterization used here is linear, and the sliding speed is the vector-valued product of basal shear stress, $-\rho gh \nabla z_s$, and a sliding constant C [e.g., Payne, 1995]. Payne [1995] advises selecting a sliding constant such that the magnitudes of the sliding and deformational velocities are similar. Vertical velocity at any level within the ice sheet, $w(z)$, is the sum of horizontal deformation of the

ice below that elevation and vertical velocity at the base of the ice sheet:

$$w(z) = - \int_{z_b}^z \left(\frac{\partial u}{\partial x} + \frac{\partial v}{\partial y} \right) dz' + u(z_b) \frac{\partial z_b}{\partial x} + v(z_b) \frac{\partial z_b}{\partial y} + \dot{b} + \frac{\partial z_b}{\partial t}. \quad (2c)$$

The terms $u(z_b)(\partial z_b/\partial x)$ and $v(z_b)(\partial z_b/\partial y)$ describe the flow of ice up or down the bed slope. Time changes in bed elevation, $\partial z_b/\partial t$, are the result of isostatic adjustment to changing ice sheet thickness.

Ice shelves flow by gravity driven horizontal spreading. In the model this is described by a set of simplified equations:

$$\frac{\partial}{\partial x} \left[2\nu_e h \left(2 \frac{\partial u}{\partial x} + \frac{\partial v}{\partial y} \right) \right] + \frac{\partial}{\partial y} \left[\nu_e h \left(\frac{\partial u}{\partial y} + \frac{\partial v}{\partial x} \right) \right] - \rho g h \frac{\partial z_s}{\partial x} = 0 \quad (3a)$$

$$\frac{\partial}{\partial y} \left[2\nu_e h \left(2 \frac{\partial v}{\partial y} + \frac{\partial u}{\partial x} \right) \right] + \frac{\partial}{\partial x} \left[\nu_e h \left(\frac{\partial u}{\partial y} + \frac{\partial v}{\partial x} \right) \right] - \rho g h \frac{\partial z_s}{\partial y} = 0, \quad (3b)$$

in which ν_e represents the effective viscosity of ice. The first term in each of equations (3) describes longitudinal strain rates. The second term describes horizontal shear-strain rates. The third term, involving ice thickness and the surface elevation gradients, describes the pressure gradient due to gravity. Vertical velocity is determined as in equation (2c), but the vertical integral is unnecessary. The ice shelf surface elevation is determined by flotation:

$$z_s = \left(1 - \frac{\rho}{\rho_w} \right), \quad (4)$$

where the subscript w denotes seawater. The equations have been derived by several authors [e.g., *MacAyeal and Thomas, 1982*]. The derivations use the dynamic boundary conditions of a stress free top surface and pressure due to seawater applied at the base and along the seaward front of the ice shelf. The seaward condition is simplified by ignoring near-field, three-dimensional effects and applying a depth-integrated seawater pressure force along the front. The simplifying assumption, that horizontal flow is depth-independent, is valid as long as the vertical length scale of the ice is much smaller than the horizontal length scale. Equations (3) are solved for ice velocity by iteration on the effective viscosity.

The constitutive relation for ice is applied in the effective viscosity term ν_e , using, as in the inland case, Glen's flow law for ice and the incompressibility condition. It is defined using a temperature-dependent rate constant \bar{B} and the flow law exponent n :

$$\nu_e = \frac{\bar{B}}{2 \left[\left(\frac{\partial u}{\partial x} \right)^2 + \left(\frac{\partial v}{\partial y} \right)^2 + \frac{1}{4} \left(\frac{\partial u}{\partial y} + \frac{\partial v}{\partial x} \right)^2 + \frac{\partial u}{\partial x} \frac{\partial v}{\partial y} \right]^{\frac{n-1}{n}}}. \quad (5)$$

The rate constant is a depth averaged value

$$\bar{B} = \frac{1}{h} \int_{z_b}^{z_s} B^{-\frac{1}{n}} dz, \quad (6)$$

taken to be uniform throughout the ice shelf. There is considerable variation in \bar{B} in modern ice shelves [*MacAyeal and Thomas, 1982*]. However, the stress balance portion of this model has successfully reproduced the flow of the Ross Ice Shelf using a spatially constant rate constant, so the assumption of constant \bar{B} seems valid [*MacAyeal et al., 1996*].

The combination of weak basal till and basal water pressure near the ice-overburden pressure results in ice stream flow that is similar to the flow of the floating ice shelf [*MacAyeal, 1989*]. As in the ice shelf, driving stress is resisted mainly by shear at the horizontal margins of the ice stream. However, unlike the ocean water beneath the ice shelf, the ice stream bed does provide some resistance to the flow of overlying ice in addition to the lateral resistance provided by the margins and the backpressure provided by the ice shelf. That resistance may arise from shear deformation within the till layer or from bed asperities protruding into the base of the ice. Here, basal flow resistance is embodied by a vector-valued basal stress term $-\mathbf{u}\beta$ added to the horizontal stress balance equations (3) in which β is a basal friction parameter (e.g., β^2 of *MacAyeal et al., [1995]*). For example, the x direction ice stream stress balance equation for ice stream flow is:

$$\frac{\partial}{\partial x} \left[2\nu_e h \left(2 \frac{\partial u}{\partial x} + \frac{\partial v}{\partial y} \right) \right] + \frac{\partial}{\partial y} \left[\nu_e h \left(\frac{\partial u}{\partial y} + \frac{\partial v}{\partial x} \right) \right] - \rho g h \frac{\partial z_s}{\partial x} - u\beta = 0. \quad (7)$$

MacAyeal [1989] and *Barcilon and MacAyeal [1993]* demonstrate that the z dependent effects of ice/bed coupling are limited to a thin boundary layer and can be ignored in the present application.

The ice stream stress balance formulation used here was derived with the view that linear viscous deformation in the basal till gives rise to the ice stream flow style [*MacAyeal, 1989*]. However, it is not necessary that the basal stress term represent till deformation. In essence, β is an operator used to reduce ice stream velocity and can be thought of as representing friction due to variations in bed shape, basal water layer thickness or basal till saturation, or bedrock asperities protruding into the base of the ice stream. Linking such effects to ice velocity implies some amount of coupling between the ice stream and its bed, a likely circumstance. Basal resistance, investigated by observation of ice motion and of the physical properties of subglacial till, has been suggested to supply anywhere from 0% to 50% of the

driving stress on Ice Stream B [e.g., *Echelmeyer et al.*, 1994; *Jackson and Kamb*, 1997; *Whillans and Van der Veen*, 1997]. In model experiments where $\beta = 0$ (zero, no basal flow resistance), the ice streams flow an order of magnitude too fast. Thus ice streams require some form of flow resistance in addition to resistance from the their margins and from the ice shelf. A consequence of the present formulation's ambiguity about the source of β is that changes in β , in space or over time, cannot be modeled. Nevertheless, it is a good starting point and model experiments [*Hulbe*, 1998] have shown that while changes in the value of β affect the rate of basal melting, even large changes in β have little impact on the temperature of deep ice, and thus on whether or not model ice streams flow.

2.5. Heat Balance

Heat flow continuity in the ice and underlying bedrock is described by an advective/diffusive equation in the ice:

$$\begin{aligned} \frac{\partial T}{\partial t} + u \frac{\partial T}{\partial x} + v \frac{\partial T}{\partial y} + w \frac{\partial T}{\partial z} \\ = \frac{1}{\rho c} \frac{\partial}{\partial z} \left(k \frac{\partial T}{\partial z} \right) + \frac{W}{\rho c}, \end{aligned} \quad (8a)$$

and a diffusive equation in the bedrock:

$$\frac{\partial T}{\partial t} = \frac{1}{\rho_r c_r} \frac{\partial}{\partial z} \left(k_r \frac{\partial T}{\partial z} \right), \quad (8b)$$

in which T represents temperature, c represents heat capacity, k represents heat conductivity, W represents viscous heating due to ice flow, and the subscript r denotes a bedrock value. The bedrock equation is solved between the bedrock surface, z_r , a fixed depth below that surface, λ (equation (12)). A geothermal heat flux is applied as a boundary condition at $z = z_r - \lambda$. The thermal capacity and conductivity of ice are temperature dependent, according to the relationships given in the notation section.

Viscous heating occurs in the inland ice sheet, where the horizontal shear stress is nonzero. It is the product of the strain rate and deviatoric stress tensors, which, according to the assumption that longitudinal stress may be neglected, is written

$$W(z) = (\rho g)^4 2 (\nabla z_s \cdot \nabla z_s)^2 (z_s - z)^4 EA. \quad (9)$$

2.6. Boundary Conditions

Several boundary conditions, in addition to those applied in the derivations, are needed to solve the balance equations. Kinematic boundary conditions consider ice flux at horizontal boundaries of the model domain and at the ice sheet surface, and motion of the ice/bed interface due to isostatic adjustment of the bedrock. Dynamic boundary conditions are needed at the nonfront exterior margins of the ice shelf and beneath the ice streams. Thermal boundary conditions constrain ice surface temperature, geothermal heat flux at the base

of the bedrock layer, and the internal boundary between ice and bed.

2.7. Kinematic Boundary Conditions

Both inflow and outflow boundaries require fixed conditions. An ice inflow boundary condition, consisting of ice volume and velocity through the boundary, must be applied at the grounded, horizontal intra-ice sheet boundaries of the model domain. A zero-flux condition is used where a model domain boundary is selected along a topographic divide, with the expectation that the boundary corresponds to the ice flow divide. A zero-flux condition is also used where a model boundary lies along a bedrock boundary, such as an ice shelf bay sidewall (i.e., along the Transantarctic Mountains (TAM)). An ice outflow condition is applied at the seaward edge of the ice shelf, such that whatever ice arrives at the shelf front must flow outward, through it. That is, a fixed shelf front position is specified and calving processes are not described. An additional flux condition is specified at the boundaries between flow regimes. At those boundaries, continuity is maintained by specifying that mass flux must be conserved across the transition line between, for example, inland ice and ice stream ice.

Kinematic boundary conditions are also specified at the upper and lower surfaces of the ice sheet. First, the rate of new ice accumulation at the upper surface of the ice sheet may be specified at a fixed value or may be computed using a climate parameterization. Simple parameterizations developed for Antarctica [e.g., *Huybrechts and Oerlemans*, 1988, 1990] that emphasize the dependence of accumulation rate on surface temperature cannot reproduce the sensitivity of West Antarctic snow accumulation to local meteorology (e.g., the effect of snow scouring due to katabatic winds blowing downslope, over the ice stream region [*Bromwich*, 1984]). Here the surface accumulation rate is specified using present-day observed accumulation rates compiled by the British Antarctic Survey [*Vaughan et al.*, 1999]. Errors in the surface accumulation rate can strongly affect the vertical heat flux and thus, ice temperature (*Fastook*, [1987] discusses the effect on basal temperature and basal melting rate; *Hulbe* [1998] discusses the relationship between surface accumulation rate and heat flux). Second, the basal accumulation rate beneath the ice shelf may be specified according to the output of an oceanographic model or by some simpler assumption. We assume an ice shelf basal melting rate of zero because no such model is available. Third, isostatic adjustment of the bedrock to changing ice sheet volume must be determined. A simple diffusion equation is used

$$\frac{\partial z_r}{\partial t} = D_a \nabla^2 \left(z_r - z_o + \frac{\rho}{\rho_a} h \right) \quad (10)$$

that describes the vertical motion of the bedrock surface, z_r , relative to the unloaded, equilibrium elevation of the bedrock surface, z_o , due to flow of the astheno-

sphere [e.g., *Oerlemans and van der Veen*, 1984]. D_a and ρ_a represent the diffusivity and density of the asthenosphere. Beneath the floating ice shelf, equation (10) is modified by replacing the weight of ice above the bedrock with the weight of water above the bedrock.

2.8. Dynamic Boundary Conditions

Two dynamic boundary conditions are defined within the model. First, a no-slip condition is applied where ice influx is zero around the perimeter of the ice shelf. Neglecting depth dependent pressure effects at ice shelf boundaries is appropriate because such effects are winnowed within an ice thickness of the boundaries [*Barcilon and MacAyeal*, 1993], which is below the resolution of the models used here. Second, flow resistance must be applied at the base of the ice streams. That resistance is embodied in the basal friction parameter β (equation (7)). As the magnitude of β increases, ice stream velocity decreases. An inverse modelling study of Ice Stream E [*MacAyeal et al.*, 1995] predicted spatial variations in basal friction with a wavelength similar to the surface topography and computed an optimal mean value for β of 1.8×10^9 Pa s m^{-1} . The observation that the onset to Ice Stream D is diffuse, with a gradual speed up occurring over tens of kilometers [*Chen et al.*, 1998], along with the more general observation that ice stream speed increases downstream despite decreasing driving stress [*Alley and Whillans*, 1991] suggests that β should vary along the course of each ice stream, being largest at the onset and decreasing downstream. The appropriate value of β is also likely to vary from ice stream to ice stream and over time due to differences basal geology and hydrology.

2.9. Thermal Boundary Conditions

Temperature must be specified at horizontal boundaries where ice flows into the horizontal boundaries of the model domain, at the upper surface of the ice sheet, at the base of a bedrock layer beneath the ice sheet, at the base of the ice shelf, and in some locations at the internal boundary between bedrock and grounded ice.

As with the ice surface accumulation rate, surface air temperature in West Antarctica is dependent on local meteorology and cannot be predicted using a simple empirical parameterization. Here, surface temperature is specified using present-day observational data [e.g., *Giovinetto et al.*, 1990].

The basal temperature condition is supplied by a geothermal heat flux G at the bottom of a layer of bedrock below the model ice sheet:

$$\frac{\partial T}{\partial z} = -\frac{G}{k_r}, \quad (11)$$

where $\partial T/\partial z$ is the bedrock temperature gradient. The bedrock layer thickness is chosen based on the e -folding penetration depth for temperature oscillations at the ice/bedrock interface:

$$\lambda = \left(\frac{2k_r}{\rho_r c_r \omega} \right)^{\frac{1}{2}} \quad (12)$$

where $k_r/(\rho_r c_r)$ is the thermal diffusivity of the bedrock and ω is the temperature oscillation frequency [*Carlson and Jaeger*, 1988]. This provides thermal inertia to the basal temperature. We select a moderately large geothermal heat flux of 0.0669 W m^{-2} for West Antarctica (a gradient of 0.02 K m^{-1} ; fluxes estimated from temperature gradients in ice boreholes range from 0.06 to 0.071 W m^{-2} ; [*Gow et al.*, 1968]; R. Bell, personal communication, 1998). The ice shelf basal temperature is fixed assuming that the ice/ocean interface is at the local pressure-dependent melt temperature. This simple boundary condition is appropriate in lieu of a ocean circulation model that would predict the temperature and salinity of ocean water at the base of the ice shelf.

Internal boundaries between bedrock and grounded ice must also be considered, and in some cases, a thermal boundary condition must be applied. The model thermodynamics include a material constraint that ice never warms above its pressure melting temperature. When warming migrates up from the ice/bed interface into the ice sheet, "polythermal ice," a mixture of ice and water at grain boundaries develops. Such conditions typically occur where shear strain, and thus viscous heating, is large. A numerical treatment of polythermal conditions has been developed by *Greve* [1995] but is not applied in the present model. Instead, it is assumed that ice reaches the melting temperature only at the ice/bed interface. That assumption is not well-justified, although it is noted that when *Greve's* polythermal model, which does not treat ice streams explicitly, is used to simulate WAIS ice flow, it predicts polythermal ice primarily in the area of present-day ice streams (R. Greve, personal communication, 1998).

The decision to fix the basal ice temperature at the local, pressure melting point, and the computation of the basal freezing rate, if applicable, is made by evaluating the heat flux at the ice/bed interface. Heat flux from the ice/bed interface into the ice above is:

$$H_o = -k \left. \frac{\partial T}{\partial z} \right|_+, \quad (13)$$

in which $\partial T/\partial z|_+$ is evaluated using the temperature at the two vertical nodes just above the ice/bed interface. Heat flux into the ice/bed interface from the rock below and heat generated at the interface from friction and freezing is

$$H_i = -k_r \left. \frac{\partial T}{\partial z} \right|_- + W_b + \frac{\rho \dot{b}}{L_f}, \quad (14)$$

where, $\partial T/\partial z|_-$ is evaluated using the temperature at the two vertical nodes just below the ice/bed interface. W_b is the heat production rate per unit area of the ice/bed interface associated with basal sliding. For the ice stream, $W_b = \beta \mathbf{u}(z_b) \cdot \mathbf{u}(z_b)$, and for the inland

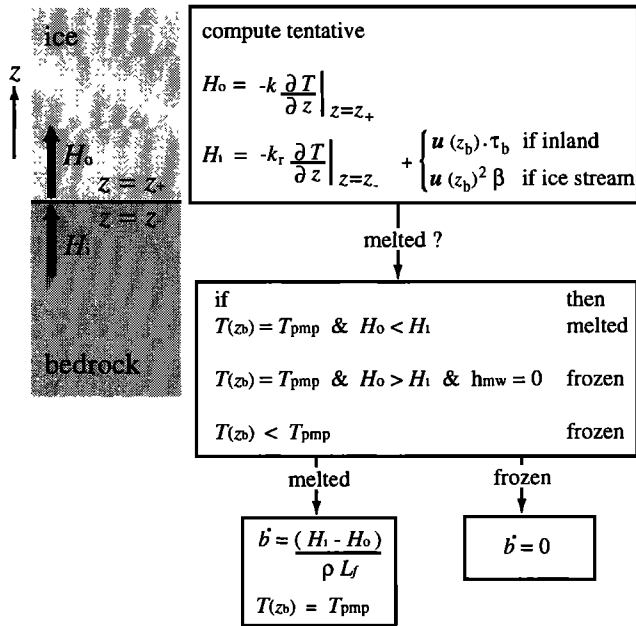


Figure 1. The model uses a sequence of calculations and logic to identify mesh nodes where basal ice is at the melt temperature. First, H_o , the heat flux out from the ice toward the ice/bed interface ($z = z_+$) and a tentative H_i , the heat flux into the ice from the ice/bed interface ($z = z_-$) including frictional heating, are computed. The decision to melt, made next, uses two criteria. If the basal ice temperature $T(z_b)$ is at the pressure melting point T_{pmp} , then the interface may be melted and the heat flux at the boundary is also considered. Where $T(z_b) = T_{pmp}$ and $H_o \leq H_i$ the interface is melted. Where the temperature criterion is met but the heat flux criterion is not, the interface, which must have been melted in the last time step, changes to the frozen state. Where $T(z_b) < T_{pmp}$, the interface must be frozen. The constraint that ice never warm above the pressure melting point is enforced by setting the temperature to T_{pmp} at all nodes where $T(z_b) \geq T_{pmp}$. The basal melt rate \dot{b} is computed where the bed is melted, using the heat flux terms and latent heat of fusion for water. In the drained-bed model, only basal melting rates (negative \dot{b}) are allowed.

ice sheet, $W_b = \mathbf{u}(z_b) \cdot \boldsymbol{\tau}_b$, where $\mathbf{u}(z_b)$ is the velocity of basal ice, which can be nonzero where basal ice is at the melting temperature, and $\boldsymbol{\tau}_b$ represents the basal shear stress (and is treated as a vector quantity). Positive \dot{b} corresponds to a basal freezing condition. Basal freezing can contribute to H_i under two circumstances, and only when $T(z_b) = T_{pmp}$. The first circumstance is when heat flow from the rock below and frictional heating exceed H_o . In this circumstance, there is basal melting and $\dot{b} < 0$. The second circumstance is when heat flow from the rock below and frictional heating fall short of H_o , but water is available at the bed for freezing, i.e., when the thickness of liquid water stored in the basal till or at the ice/bed interface, h_{mw} , is greater than zero. In both circumstances, \dot{b} is computed by

$$\dot{b} = \frac{k_r \left. \frac{\partial T}{\partial z} \right|_- - k \left. \frac{\partial T}{\partial z} \right|_+ - W_b}{\rho L_f}, \quad (15)$$

where subscripts + and - denote evaluation of vertical derivatives above or below the interface, respectively. Changes in h_{mw} over time require a model of basal water flow. Such a model is under development, but here the bed is assumed to be instantaneously drained. That is, h_{mw} is always zero.

Equations (13), (14) and (15) are interdependent. Computation of H_i (equation (14)) requires knowledge of \dot{b} (equation (15)), which itself requires knowledge of H_i (equation (13)). An information impasse is averted by breaking the computation into a sequence of steps that use a logical evaluation to determine the basal melting or freezing state. That process is shown in Figure 1 and described in the caption.

2.10. Flow Regime Boundaries

The model performs a series of logical evaluations in order to determine where the inland ice, ice stream, and ice shelf equations are to be applied. Floating ice is identified by comparing the bedrock surface elevation z_r with the elevation $z_b = z_{sl} - \rho h / \rho_w$ of the ice bed if the ice column were to be floating, where z_{sl} represents the sea surface elevation. Model mesh nodes for which the inequality:

$$z_r < z_{sl} - \frac{\rho}{\rho_w} h \quad (16)$$

evaluates true are assigned ice shelf status. All other nodes are identified as grounded ice. This method of node classification allows the model to determine the position of the boundary between grounded and floating ice so the grounding line is free to migrate according to changes in ice thickness over time.

Inland ice and ice stream nodes are subsets of the group of grounded ice nodes. Ice stream nodes are predefined in the model setup, and all other grounded nodes are assigned inland ice status. An alternative would be to classify regions within the model domain according to bedrock geology and to use the presence of till and the basal temperature condition $T(z_b) = T_{pmp}$ to assign ice stream status. Such a scheme cannot be employed at present because knowledge of the spatial variation of bedrock type is limited but can be added to the model in the future, as more airborne geophysical data become available [cf. *Bell et al.*, 1998].

2.11. Model Implementation

The finite element method is used to solve the partial-differential equations that describe ice sheet dynamics and thermodynamics. Horizontal equations are represented by piecewise linear functions on a two-dimensional triangular mesh that represents a map view of the model domain (Figure 2). Vertical balance equations are represented by linear functions along one-dimensional arrays of nodes that descend beneath the horizontal mesh

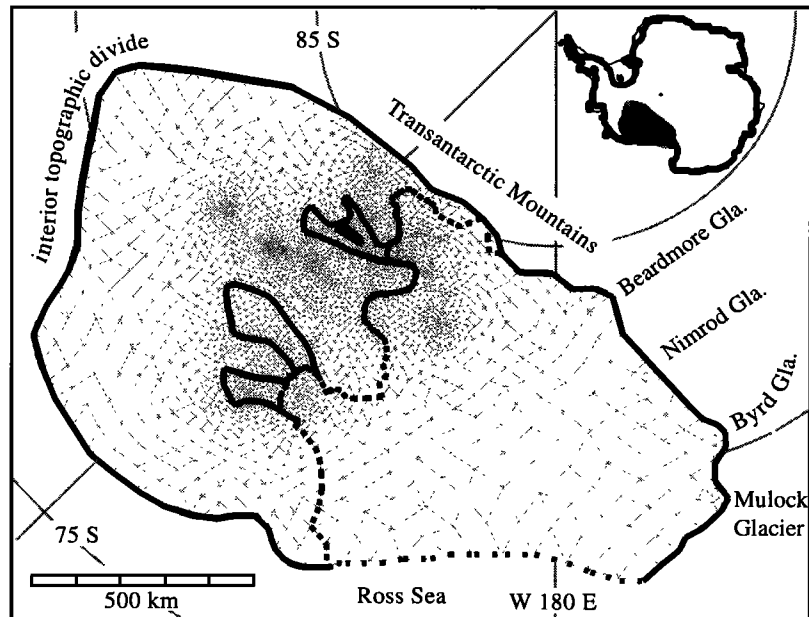


Figure 2. The model domain encompasses the Ross ice streams, their mass catchment basins, and the Ross Ice Shelf, into which the ice streams flow. Accordingly, the exterior boundary follows the topographic divide of the inland ice sheet from the coastal mountains of Marie Byrd Land to the Transantarctic Mountains and traces along both mountain ranges to the Ross Ice Shelf front. The shelf front boundary (dotted line) approximately follows the pre-1989 shelf front position. The heavy line denotes the outlines of Ice Streams B, D, and E (named right to left). Ice inflow is specified for the four identified Transantarctic Mountain glaciers. The domain is divided into 6229 triangular elements, which corresponds to 3168 triangle vertex nodes. Mesh resolution is finest in the ice stream region, where the minimum element area is 4.21 km^2 . Resolution is coarsest in the ice shelf, where the maximum element area is $3.28 \times 10^3 \text{ km}^2$. Twenty-six vertical layers are specified, 21 of which are in the ice and 5 of which are in the bedrock. The vertical nodes are spaced logarithmically in the 9 lowest layers of ice, such that resolution is maximized near the base of the ice sheet and linearly elsewhere.

nodes. Model variables are defined and computed at mesh nodes (triangle vertices) and gradients thereof are computed within each triangular element. Most of the equations are solved using linear interpolation within the mesh "elements." Higher-order interpolation is required to compute mass flux in the inland ice (e.g., the second derivative of the surface elevation must be computed within each mesh element). A complete discussion of casting the model equations in a finite element form is given by Hulbe [1998] [see also Fastook, [1987]; D. R. MacAyeal, Lessons in ice sheet modelling, unpublished manuscript, 1998].

The finite element method offers two important advantages over the more common finite difference method. First, because integral equations are solved instead of differential equations, flow regime boundaries do not present an obstacle that must be parameterized or omitted as is the case for finite difference methods [cf. Hindmarsh, 1993; Huybrechts, 1990]. Second, mesh resolution can vary. Variable resolution allows the model to accommodate many length and velocity scales within one domain and to focus computational effort on areas of special interest.

An important consideration in model implementation, and perhaps the greatest limitation to the present model, is the length of model time between each calculation, the time step size Δt . Ideally, Δt should be as long as possible and should conform to the timescales of change in the variables being computed. For example, ice thickness evolves slowly so it would be efficient to take large time steps between mass balance calculations. In practice, time step size is limited by numerical "noise," node-to-node variation in a quantity that arises due to instability in the model numerics. In the present model the nonlinearity of the ice flow law can cause such instability. One solution to the problem is to select a small Δt for mass and stress balance calculations. The appropriate Δt depends on geometry and on ice velocity. In general, Δt should be small enough so that any particle of ice cannot transit through more than one element in any time step. This prevents sudden changes in thickness at mesh nodes that will be amplified by the nonlinear flow law and will result in node-to-node noise. Another solution to the problem of numerical noise is to apply some form of artificial damping to small-scale variations in ice thickness. This is a cosmetic technique

that smoothes the computed fields but does not affect the underlying cause of the noise. Here, artificial damping is avoided by the selection of a small Δt .

The processes of heat balance operate on much longer timescales than the time step length required for stability in the mass and stress balance calculations (tens to hundreds of years versus hundredths of years). Computing new ice temperatures at every mass and stress balance time step would be inefficient. Asynchronous time steps are used here to facilitate the two different timescales. While the other balance equations are solved at every time step, the heat balance equations are solved less frequently.

2.12. Model Initialization

A model domain encompassing the Ross ice streams, their catchment areas, and the Ross Ice Shelf is used to demonstrate the numerical model (Figure 2). The domain may be initialized by one of several commonly used forward methods [cf. *Huybrechts and Oerlemans*, 1990, 1988; *Payne*, 1995; *Payne and Dongelmans*, 1997]. The best option is to begin from a minimally glaciated state and to allow the ice sheet to “spin up” through a glacial climate cycle toward the present-day using regional climate records. Unfortunately, the quadratic interpolation method used to accurately compute mass flux in the inland ice and the small time step size needed to ensure numerical stability make a climate-cycle spin-up computationally impractical for the present model. Thus we use an alternative initialization procedure and assume that the present-day observed ice sheet geometry approximates a steady state. Starting with the observed ice sheet geometry, the model is used iteratively to find a thermal and mass balance steady state for the given domain and boundary conditions. If the assumption of a near-steady state starting point is correct, the fully initialized ice sheet geometry should be similar to the starting geometry. Some details, especially in ice temperature, will be missing because the initialized ice sheet state has no memory of past climate events.

Initial ice surface elevation and thickness and bedrock elevation are interpolated to the node points of the finite element mesh from gridded data from the Scott Polar Research Institute Antarctic glaciologic folio [*Drewry*, 1983]. The observational data used to construct the folio maps and grids have variable coverage and error so the initialization is also of variable quality. For example, coverage is sparse over northern Marie Byrd Land and some shorter-wavelength features, such as small mountains, may not be represented in the bedrock topography data. Ice sheet surface elevation data are more robust because the surface shape changes over longer distances and in a more predictable way than does the shape of the bedrock surface. The model map projection is polar stereographic with standard parallel 71°S. This is a common projection for Antarctic Ice Sheet models and data maps.

Selection of a domain exterior that corresponds with the ice flow divide for most of its length simplifies the horizontal boundary conditions. Ice flow across the divide is zero so the ice flux boundary condition is zero and no inflow ice temperature is required. Ice inflow is specified for Mulock, Byrd, Nimrod, and Beardmore Glaciers (290, 740, 150, and 330 m yr⁻¹, respectively, from *MacAyeal et al.*, [1996]), the largest glaciers flowing into the ice sheet from the TAM. Ice thickness is fixed at those inflow boundaries using observed grounding line thickness. Elsewhere along the exterior boundary, ice thickness is allowed to vary according to mass balance, with the condition that surface slope is zero (i.e., it is assumed that the flow divide remains spatially and temporally fixed).

Several considerations prompt predefinition of the regions in which ice stream flow is possible. First, the spatial distribution of the unconsolidated sediments (i.e., till) is only approximately known. Second, the degree of water saturation of those sediments and the nature of the water drainage system at the ice/bed interface are not well-constrained. Third, the ice dynamics only version of the model tested here does not include balance equations for either the basal till or water. Thus the model has limited information with which to decide where ice streams should or should not flow. Instead, the present-day ice stream margins are used to define regions in which ice stream flow is possible (digitized flow boundaries provided by P. Vornberger and digitized from the map of *Alley and Whillans*, [1991]). The outlines of the ice streams are smoothed somewhat, in order to moderate the number of mesh elements needed to fit the shapes of the boundaries. The upstream extent of the ice streams is inferred from the digitizations, although as noted earlier, an ice stream “onset” is difficult to define. Ice Streams A and C are assumed to flow by inland, instead of ice stream, ice dynamics. Ice Stream A flows in a distinct subglacial valley [*Shabtaie et al.*, 1987] and at slower speeds than other named ice streams and thus has more affinity to glacier flow than to ice stream flow. The main trunk of Ice Stream C is quiescent at present.

Limitations in knowledge of basal conditions also affect the selection of the basal flow resistance parameter. It is likely that basal friction varies spatially; indeed, the mismatch between observed velocities and assumed balance computed for uniform basal conditions (discussed below) implies that is the case. However, the goal here is to evaluate model performance, not to reproduce WAIS flow exactly, so selection of a spatially uniform basal friction parameter is sufficient. We select $\beta = 2.0 \times 10^9$ Pa s m⁻¹, which is close to the value determined in the inverse modeling study of basal friction in Ice Stream E by *MacAyeal et al.*, [1995].

Time step size is different for the heat balance and mass balance portions of the model. Changes in temperature occur slowly, so a large time step size, 500 years, is selected. The fine model mesh resolution in the

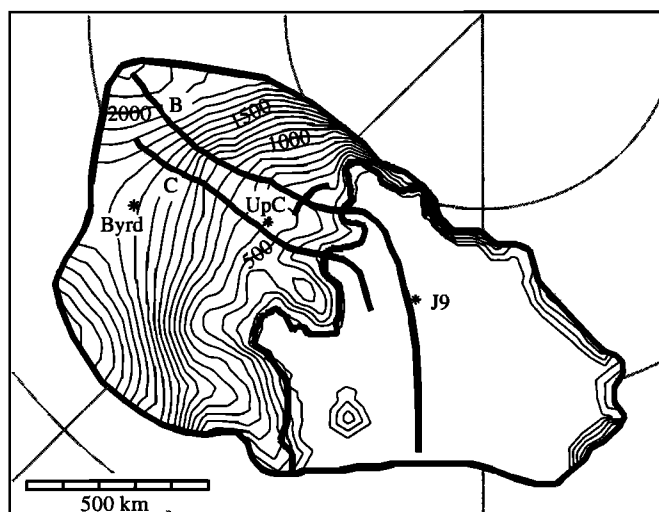


Figure 3. Locations of cross sections along which model output is presented, plotted on a map of ice surface elevation in the model domain. The contour interval is 100 m. Three sections through present-day ice streams and into the ice shelf are identified by the ice stream names. Vertical exaggeration for the downstream sections is about 133:1. One transect runs across Ice Stream B. Vertical exaggeration for the across-stream section is about 16:1. The UpB camp (not shown) lies approximately at the intersection of the two Ice Stream B sections. The locations of Byrd Station, the UpC camp, and J9 are marked with asterisks.

ice stream and grounding line areas mandates a much shorter time step, 0.05 year, for the mass balance and stress balance calculations. Each heat balance calculation requires about 2.1 min (about 364 million floating point operations) on a Sun Ultra™ Enterprise™ 2 with a 300-MHz processor and one complete cycle of stress balance, mass balance, and heat balance calculations requires from 4 to 4.3 min (about 515 million floating point operations), depending on the number of iterations within the ice shelf and ice stream stress balance solution.

3. Model Performance

Model performance is evaluated using the initial, assumed balance velocity and the thermal steady state spin-up results. Limitations inherent in the initialization technique made continuing from the thermal spin-up to a full mass balance spin-up impractical. Computed fields, such as ice temperature and velocity, are presented in plan view contour maps and in cross sections that run from the inland ice, through the ice streams, and into the ice shelf. The locations of the sections are shown on a map of the model domain in Figure 3.

3.1. Initial Velocity

Initial velocity is computed with the assumption that the present-day ice sheet and its model representation

are near a steady state mass balance. If that assumption is valid and if the stress balance model works well, the initial ice velocity should compare favorably with observed velocity. Model-computed velocity (Figure 4) is evaluated in a general sense according to common understanding of WAIS flow and by direct comparison at locations where surface velocity has been measured. Inland ice speed is, as expected, small (of the order of 10 to 50 m/yr) except where ice thickness and surface slope are large, for example, upstream of Ice Stream A, along the front of the TAM. The model accurately predicts near-zero velocity of ice in the interstream ridge separating the tributaries of Ice Stream B and the slow flow of ridges between ice streams (Figures 5 and 6). Measured and modeled surface speed are very similar at Byrd Station, about 12.7 m/yr and 13.6 m/yr, respectively, as are the measured and modeled depth variations of ice speed (Figure 7). The computed assumed balance speed of Ice Stream A is modest, about 100 m/yr, compared with measured speeds of about 220 m/yr [Shabtaie *et al.*, 1987]. The ice stream's speed may be increased by specifying boundary inflow from Reedy Glacier. However, treating A as an ice stream, instead of as inland ice, would have resulted in ice flow an order of magnitude too fast.

Many distinctive features of ice stream flow are well-represented, although, in general, the ice streams flow too slowly. The sluggishness of modeled ice streams is simply a consequence of the selection of a basal friction parameter β , which could be changed to produce faster or slower ice velocity. Adjusting β would provide more pleasing velocity magnitudes but would not be useful for evaluating model performance. A more instructive pursuit is to examine the pattern of modeled ice stream flow. Ice streams are characterized by narrow shear margins and a U-shaped across-stream velocity variation [cf. Whillans *et al.*, 1993; Whillans and

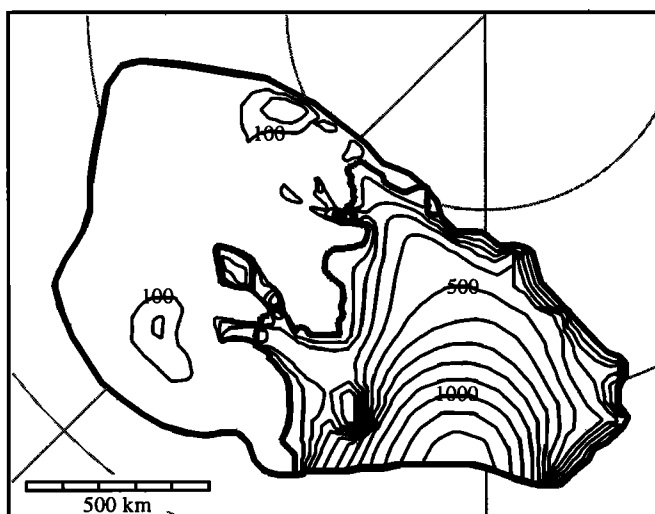


Figure 4. Initial (assumed balance) surface speed. The contour interval is 100 m/yr. Compare with Figures 2 and 3 for locations of the five WAIS ice streams.

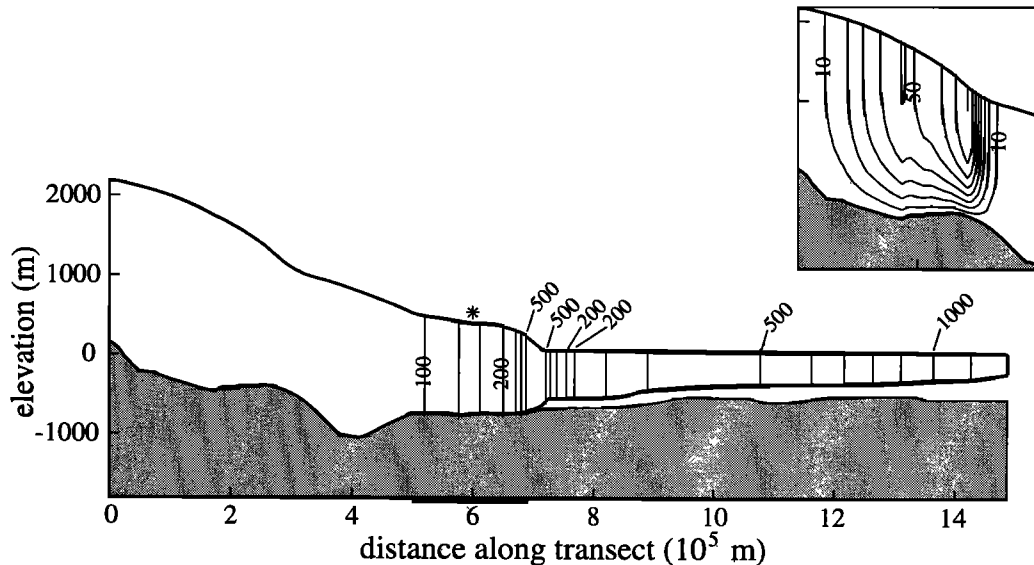


Figure 5. Ice speed in a cross section from the inland ice divide, through Ice Stream B, and to the front of the floating ice shelf. The region of ice stream flow is underscored by the heavy line. The contour interval is 100 m/yr.

van der Veen, 1997]. Those attributes are found in all the modeled ice streams. The across-Ice Stream B transect plotted in Figure 8 is a good example: horizontal speed increases from near zero at the margins to near maximum across a narrow band, and most of the interior of the ice stream flows rapidly. The observed slowdown as the ice stream flows across the grounding line and enters the ice shelf [cf. *Alley and Whillans, 1991*] is also manifest in the modeled flow, although the site of the slowdown is offset because the model-selected grounding line is upstream of the actual present-day grounding line (Figures 5 and 6). The observed contin-

uous downstream speedup from onset to grounding line is not reproduced. In the model, ice velocity decreases where ice stream thickness decreases, as is required by the continuity equations. Mismatch between measurement and model must therefore arise from inadequacies in the model-specified basal boundary conditions (e.g., β). Basal friction must not be constant but must vary along the course of Ice Stream B, decreasing where the modeled ice flow is too slow. Basal shear stress corresponding to the assumed β and resulting ice velocity agrees favorably with basal drag computed from observations on Ice Stream B [*Whillans and van der Veen,*

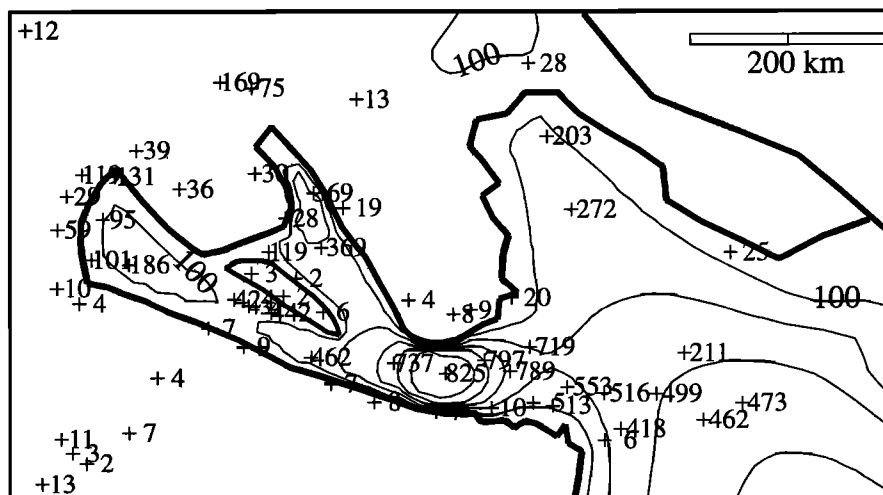


Figure 6. Comparison between model-derived and measured surface speed in the vicinity of Ice Streams A, B, and C. The model uses a uniform basal friction parameter. The contour interval is 100 m/yr. The measurements, in m/yr, are from *Whillans and van der Veen, [1993b]*. The inland ice boundary, denoted by the heavy line, outlines Ice Stream B.

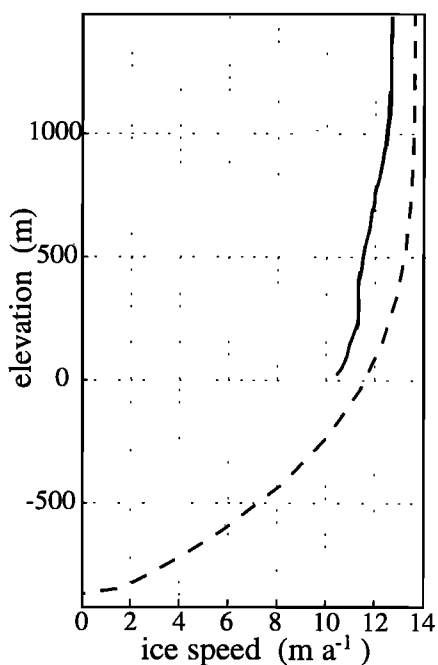


Figure 7. Depth variation of ice speed at Byrd Station, an inland ice location. The model-computed speed is plotted as a dashed line, and ice speed computed from measurements of borehole tilting is plotted as a solid line. The borehole measurements end above the base of the ice sheet because the borehole closed before the experiment was completed. The data are digitized from *Whillans* [1977]. The model speeds are for a mesh node close to Byrd Station.

1993a], with maximum values of about 389 and 60 kPa, respectively. Ice Stream E provides the best match between the pattern of observed and modeled velocity. Good agreement should be expected for Ice Stream E because it was the subject of the inverse modeling study used to estimate the model's basal friction parameter [MacAyeal *et al.*, 1995]. MacAyeal *et al.*'s [1995] study found relatively small spatial variations in basal friction. Overall, the model performs well in the ice stream areas. The challenge of reproducing observed patterns of downstream velocity change within the ice streams anticipates the model's usefulness, when combined with observational data, for studies of variations in conditions at the ice/bed interface.

Ice shelf flow is well-reproduced by the model. This is anticipated, as the ice shelf portion of the model has been validated and used in several other modeling studies [e.g., *Hulbe*, 1997; *MacAyeal et al.*, 1996]. Differences between modeled and measured ice speed are largest where there are discrepancies in inflow velocity: where the model underpredicts the rate of ice stream discharge and where flow from small outlet glaciers of the TAM has been ignored. Underpredictions in ice shelf speed can be corrected by refinements in the basal boundary conditions of the ice streams and by the addition of more inflow along the mountains. Ice shelf speed is

overpredicted downstream of Ice Stream C, where the model asserts that ice is floating but where observation would suggest the ice is partly grounded (in the area of Steershead and Crary Ice Rise). That problem is likely due to errors in the initial ice thickness or basal topography.

3.2. Thermal Equilibrium

Evaluation of the steady state ice sheet temperature computed by the thermodynamic portion of the model relies on a combination of observation, extrapolation, and common sense. The broadest picture of ice sheet temperature available is that of water at the ice/bed interface, inferred from airborne radar soundings [cf. *Shabtaie et al.*, 1987]. In general, water appears to be present beneath the active ice streams and beneath much of Ice Stream C but is not observed beneath the

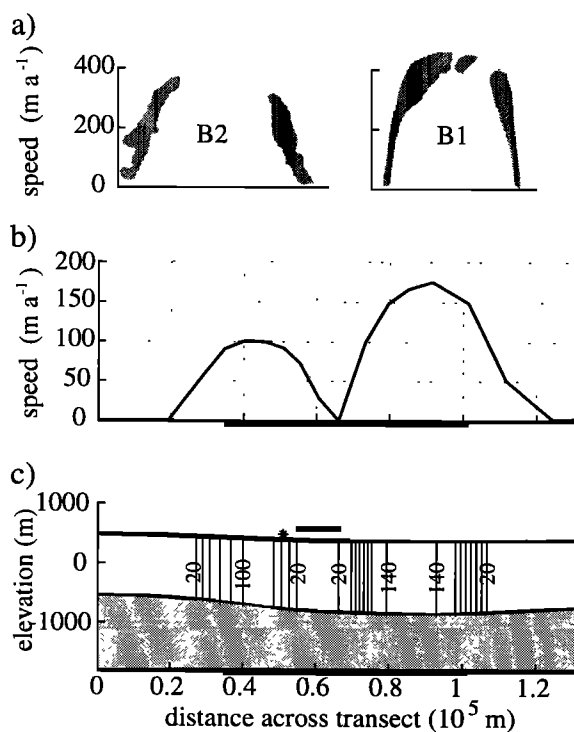


Figure 8. Ice speed in a cross section that is approximately perpendicular to the flow direction of Ice Stream B. The transect intersects the interstream ridge, which is easily identified by a sudden decrease in speed within the body of the ice stream. (a) Downstream component of velocity across the northern, B2, and southern, B1, tributaries of the ice stream, measured by crevasse tracking [after *Whillans and van der Veen*, 1997]. (b) Ice speed across the modeled stream. The shapes of the curves are similar, but the comparison is limited by the resolution of the model, about 3 km in this area. (c) The ice stream shear margins emerge as zones of rapid change in speed (close contour spacing) in a vertical view of the across-B section. The region of ice stream flow is underscored with a heavy line, the interstream ridge is underscored with a heavy line, and the location of the UpB camp is denoted by an asterisk. The contour interval is 20 m/yr.

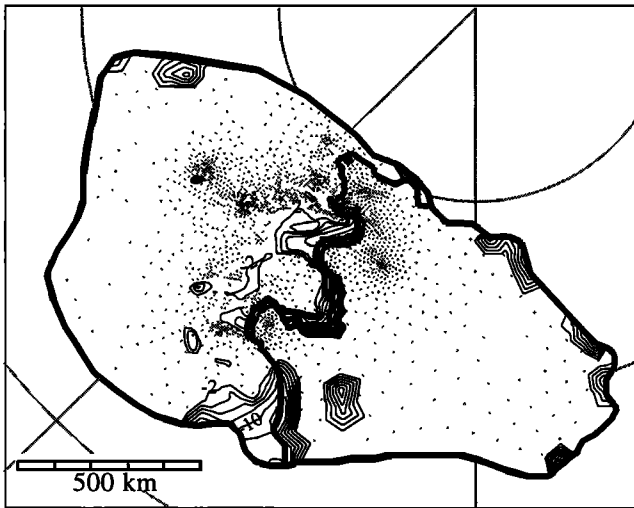


Figure 9. Homologous temperature at the bed at the end of the thermal equilibration. Homologous temperature is the ice temperature minus the pressure melting point temperature, so a negative value indicates a frozen bed. The contour interval is 2 K.

interstream ridges. Water floods into boreholes drilled on Ice Stream B, while drilling fluid (water) rushes out of boreholes drilled at the UpC camp [Engelhardt and Kamb, 1997; H. Engelhardt, personal communication, 1998]. A borehole drilled in the ridge between Ice Stream B's two tributaries found basal ice below the melt temperature (H. Engelhardt, personal communication, 1998). Basal ice temperature is of particular interest because it is important to the viability of ice streams and to the magnitude of grounded ice velocity. Also, while the initialization technique used here does not allow the model to correctly capture all features of the depth variation of ice temperature, it should be able to reproduce general features such as basal melting. More locally, borehole temperature data from Byrd Station, Ice Streams B and C, and station J9 on the Ross Ice Shelf are compared with model-computed ice temperature. The following evaluation of steady state ice sheet temperature computed by the thermodynamic portion of the model relies on a combination of observation, extrapolation, and common sense.

The homologous temperature of basal ice at model equilibrium and mesh nodes at the melt temperature at the ice/bed interface are mapped in Figures 9 and 10. The model predicts basal freezing beneath interstream ridges (Figures 10 and 11) and Siple Dome, which are expected to be frozen, according to field observations, and beneath the downstream section of Ice Stream C, which has recently ceased rapid flow and where observed temperature is near the melt temperature. Surprisingly, substantial portions of the ice streams are also predicted to be below the melt temperature at the bed (Figure 10). That result suggests that the present day geometry of the ice streams (relatively thin) promotes a tendency

toward freezing. The modeled depth-variation of temperature at the UpB and UpC borehole sites compares favorably with measured ice temperature so the model thermodynamics is sound (Figure 12). Rather, spatial variation in basal melting beneath the ice streams is due to the present-day tendency toward basal melting or freezing because the initialization technique has no memory of past conditions. Variations may also be due to the assumption of spatially uniform boundary conditions (for example, the geothermal heat flux and basal friction or lack of a meltwater storage and drainage system).

Thermal spinup of the inland ice is more problematic. The model ice sheet develops thick interior zones of ice at or near the melt temperature that are certainly incorrect. The error in the model-derived depth variation of inland ice temperature is demonstrated by a downstream cross section through Ice Stream B (Figure 13), which intersects two volumes of anomalously warm ice. Comparison of modeled ice temperature with temperatures measured in the Byrd Station borehole (Figure 12) shows a slight overthickening of warm ice near the base of the core, but for most of the depth of the core the modeled and observed temperature curves are similar. The problem does not develop within Ice Stream C (Figures 12 and 14), which is treated as inland ice in the model, so it is unlikely to be an error in the model physics. There is no inland/stream boundary in the vicinity of Ice Stream C, yet anomalous warming does occur inland of the quiescent stream so the warming cannot be due to a problem in the model numerics. The anomalous ice warming must be due to something peculiar to the geometry of the ice sheet's interior: a positive feedback between strain heating and the tem-

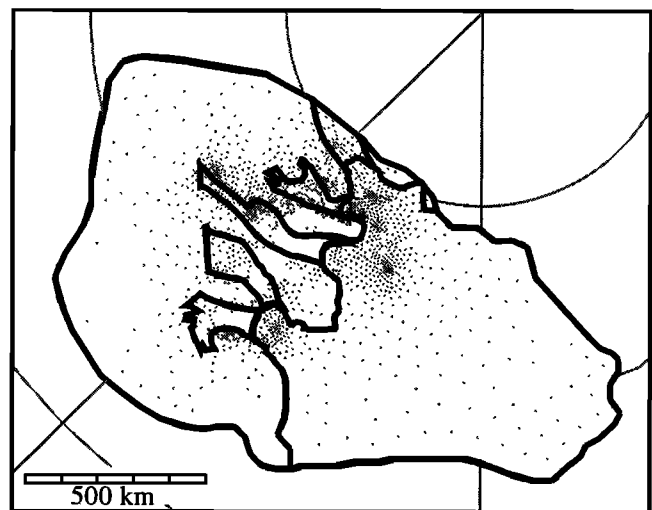


Figure 10. Model mesh nodes at the melt temperature are plotted with the approximate outlines of the five WAIS ice streams. Note that node density varies throughout the model domain, being greatest in the ice stream and grounding line areas.

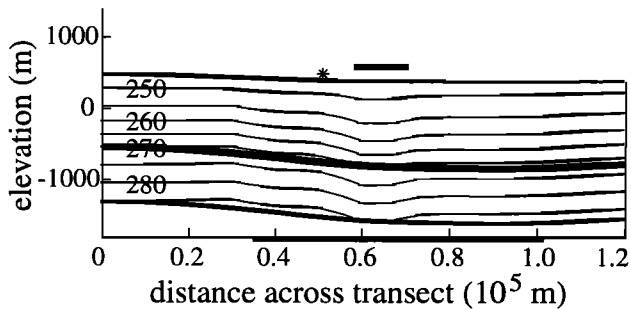


Figure 11. Ice and bedrock temperature across Ice Stream B at the end of the thermal equilibration. The contour interval is 5 K. The ice/bed boundary is drawn with a heavy line. The region of ice stream flow is underscored with a heavy line, the interstream ridge is overscored with a heavy line, and the location of the UpB camp is denoted by an asterisk. The 270 K contour dips down to the ice/bed interface beneath the interstream ridge indicating a frozen bed. This model predicted frozen bed condition beneath the ridge agrees with field observations.

perature dependence of the flow law, amplified by steep surface slope [cf. *Payne and Dongelmans, 1997*]. The correlation between surface steepening and the model's interior warm ice zones occurs everywhere and is particularly striking in a profile from the inland ice reservoir, through Ice Stream C, and into the ice shelf (Figure 14). Steep surface slope causes large shear strain rates near the base of the inland ice sheet which, in turn, produce large viscous heating. Over the course of the thermal spin-up, heating warms ice at depth with the result that the ice deforms more rapidly. When the initialization routine updates ice velocity, the faster deformation produces even larger viscous heating. The feedback continues, and a thick core of ice near the melt temperature is created. Strain heating is maximal just upstream of a surface slope break, so a steep temperature gradient develops beneath the slope break (Figure 14). Vertical velocity is strongly downward upstream of the break. Large velocity would thin the ice, were the mass balance portion of the model to be used. Indeed, the erroneous inland ice temperatures can be attributed to our requirement of fixed ice thickness during the thermal equilibration.

The importance of the strain heating feedback is demonstrated by repeating the thermal equilibration with constant, instead of temperature-dependent, flow law parameters (notation section). A flow law with parameters set for ice at 263 K suppresses the feedback and yields smooth temperature fields in the steady state ice sheet (Figure 15). Thus it is concluded that the anomalous warming is a normal result of the feedback between ice deformation and temperature in the flow law, amplified by the initialization technique.

Model-computed ice shelf temperatures are compared with temperature measured in the J9 borehole on the Ross Ice Shelf (82°22'S, 168°38'W; Figure 12). The

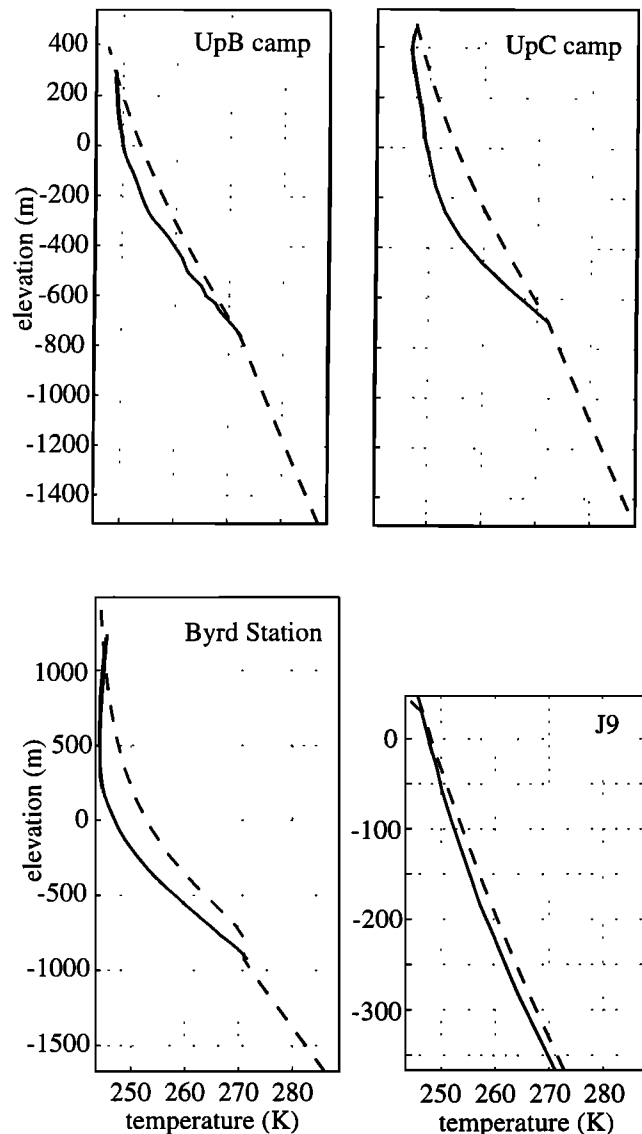


Figure 12. Comparison of model-computed and measured ice temperature at four locations: the UpB camp on Ice Stream B, the UpC camp on the now quiescent Ice Stream C, at Byrd Station in the interior of West Antarctica, and at station J9 on the Ross Ice Shelf. Measured temperatures are plotted as a solid line (from *Engelhardt et al., [1990]*, H. Engelhardt (personal communication, 1998), *Robin, [1983]*, and *MacAyeal, [1979]*, respectively). Modeled ice and bedrock temperatures are plotted as a dashed line. Small differences in the shapes of the curves at each point may be due to past variations in surface temperature and accumulation rate and in basal melting, which cannot be accounted for by the model initialization process. At the UpC site, the observed temperature at middepth is cooler than the modeled ice temperature because past basal melting, not reproduced by the initialization process, has removed warm ice from the base of the ice stream, depressing ice temperature. At Byrd Station the difference between the two curves near the ice/bed interface (about -900 m elevation) is due to the development of an overthick layer of deep inland ice at the melt temperature during the thermal equilibration process.

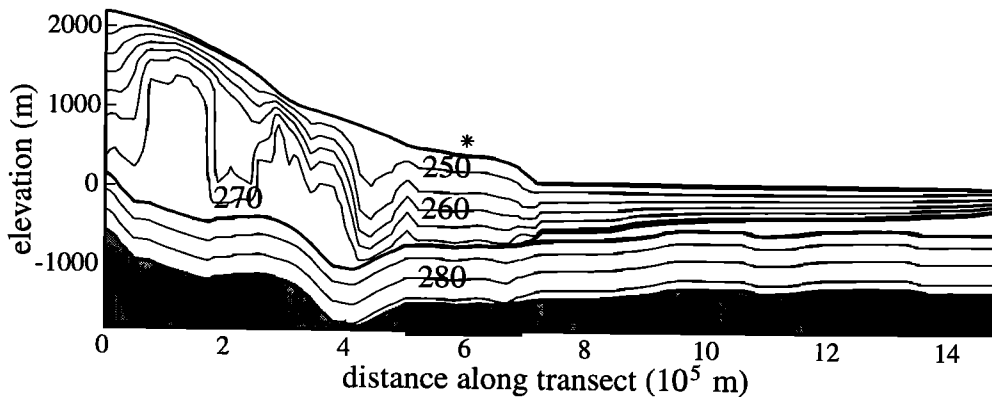


Figure 13. Ice and bedrock temperature at the end of the thermal equilibration, along the cross section that includes Ice Stream B. The contour interval is 5 K. The ice/bed boundary is drawn with a heavy line. The region of ice stream flow is underscored by a heavy line, and the location of the UpB camp is denoted by an asterisk.

shapes of the two temperature profiles are similar, and the largest difference at any depth is about 2 K. The shape of the observed temperature profile is due, in part, to the dynamic history of the ice shelf [MacAyeal, 1979]. The thermal equilibration process used here does not account for past flow or for oceanographic effects so some discrepancy between modeled and observed ice temperatures is expected.

3.3. Conclusions From the Thermal Equilibration Process

Overall, the model performs well, even without any attempt at parameter tuning. Initial, assumed balance velocities computed by the model are similar to measured surface velocities. Where differences occur, they can be explained by inadequate specification of boundary conditions and in a few places by erroneous thermal effects. In some cases, the corrections to those conditions can be made easily (such as adding inflow from small Transantarctic Mountain glaciers). In other cases (such as ice stream basal friction), improved boundary conditions require additional research.

The thermal equilibration process worked well in the ice stream area and in the ice shelf but worked poorly in some inland ice locations. The initial intent was to follow the thermal spinup with a full mass, stress, and heat balance equilibration. Such a procedure would eventually correct temperatures in the inland ice. The European Ice Sheet Modelling Initiative (EISMINT) Phase II, Level 2 model validation is similar to the full initialization intended here so experience from the EISMINT validation of the present model (discussed in section 3.4) can be used to predict the sequence of events were a full equilibration to be performed. Rapid discharge of the warm ice would thin the inland ice and allow it to cool. Ice sheet volume would decrease rapidly, falling below the volume that corresponds to a balance situation for the present-day boundary conditions. The thin,

cool, slow flowing ice sheet would then regrow slowly toward steady state. Such an equilibration process requires thousands of model years to reach steady state and is thus not practical for the high-resolution WAIS model and available computational resources.

The development of thick, warm ice zones during the thermal equilibration of the model is an exaggeration of a real process within the WAIS. Curiously, the surface steepening and related ice warming occurs near the present-day ice stream onsets. The steepening must be, in part, a consequence of faster ice discharge downstream of an ice stream onset, but that steepening may also play an important role for the onset, warming ice to the point where basal sliding, and in turn, frictional heating and basal meltwater production, can begin. Once an acceptable initialization method is established, the whole-ice-sheet model will be well-suited to explore ice stream onset processes.

3.4. Model Validation

The European Ice Sheet Modelling Initiative has established formal guidelines for the validation of numerical ice sheet models. The numerics of the present model are validated according to the EISMINT Phase II, Level 2 control experiment (P. Huybrechts, <http://homepages.vub.ac.be/~phuybrec/eismint/antarctica.html>). This is a whole Antarctic ice sheet test in which models are simplified so that the comparison will not be affected by special preferences of individual modelers. The present model, fitted to the EISMINT intercomparison design, performs well over the long iteration process. Changes in grounding line location, including the brief development of isolated areas of floating ice surrounded by grounded ice, are handled smoothly and do not cause instability in the model. Areas of excessively fast flow, due to limitations in the input data, do not cause numerical instability. Such areas simply discharge a large volume of ice until they thin sufficiently

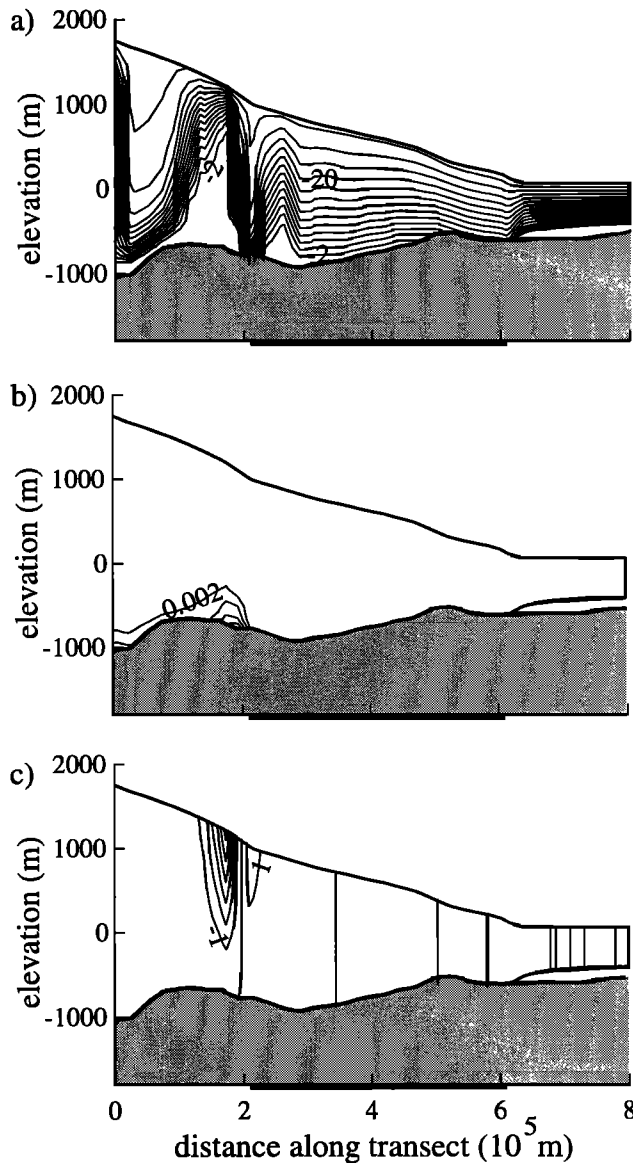


Figure 14. (a) Homologous temperature, (b) viscous heating, and (c) vertical velocity in the ice along a cross section from the inland catchment, down Ice Stream C, and into the ice shelf. The contour intervals are 2 K, 1 m/yr, and 0.002 W m^{-2} , respectively. Negative vertical velocity indicates ice moving downward, upstream of the nickpoint. The slope break and large strain heating occur near the head of the now stagnant ice stream.

to reach steady state or over thin and then regrow to steady state. We conclude that the model behaved as expected, indicating no errors in the underlying numerics.

3.5. Discussion

This present contribution offers a new three dimensional, finite element, dynamic/thermodynamic numerical model of ice sheet, ice stream and ice shelf dynamics. Advances over past work include the coupling of ice stream, inland ice, and ice shelf physics into one

quasi-three-dimensional model and the incorporation of both vertical and horizontal temperature advection into the thermodynamics. Modeled present-day ice flow and temperature, used to evaluate model performance, compare favorably with observation. Discrepancies that exist are due in part to limited knowledge of some boundary conditions and to flaws in the chosen initialization technique.

The principal limitation in applying the numerical model is computation time. Our preferred method for computation of surface elevation gradients from elements to nodes, Gaussian quadrature, (used for inland ice mass flux calculations) is computationally intensive, precluding long time span experiments. Long computation time is also a hurdle for model initialization, limiting the model's use to certain types of problems (i.e., studies of ice stream and ice shelf flow coupled to a steady state inland ice sheet; studies in which the flow law parameters for inland ice are specified for a cold temperature; studies of present-day ice sheet interaction with the bed). An effort to reconfigure the model to use a fast linear interpolation only scheme is now underway. Experiments with centroid based Delaunay triangulation yield unreasonable interpolated values where gradients change significantly over length scales similar to mesh resolution and interpolation error can be dependent on mesh geometry. An approach which holds more promise capitalizes on the nearly 2 to 1 ratio of elements to nodes for large triangular meshes. The problem of interpolating from element centers to nodes is thus overdetermined and appropriate for a least squares inversion. If a linear interpolation scheme is adopted, its inherent smoothing will affect model accuracy. Such smoothing is unlikely to affect the outcome of long-time ice flow simulations but could be important to detailed investigations. A lower-order model could be restricted to use in model initialization, and the higher-order model could be used for experimentation.

The challenge of improving model initialization is largely technical. Once those improvements are made, the model will be a good investigative and prognostic tool. However, even the anomalies produced by an inadequate initialization technique contain information. Although the effect of steep changes in surface slope on strain heating and ice temperature was amplified in the model results discussed here, that heating is required by the thermodynamics of ice flow and is probably related to the inland onset of ice streams.

The challenge of improving boundary conditions is the challenge of understanding how the ice sheet system works. For example, the model ice streams flow an order of magnitude too fast when there is no coupling between ice and the till over which it flows, implying that ice streams require some form of flow resistance in addition to resistance from the their margins and from the ice shelf. That resistance may be provided by basal friction, as modeled here, or could be due to some other manner of interaction between ice and bed, or by

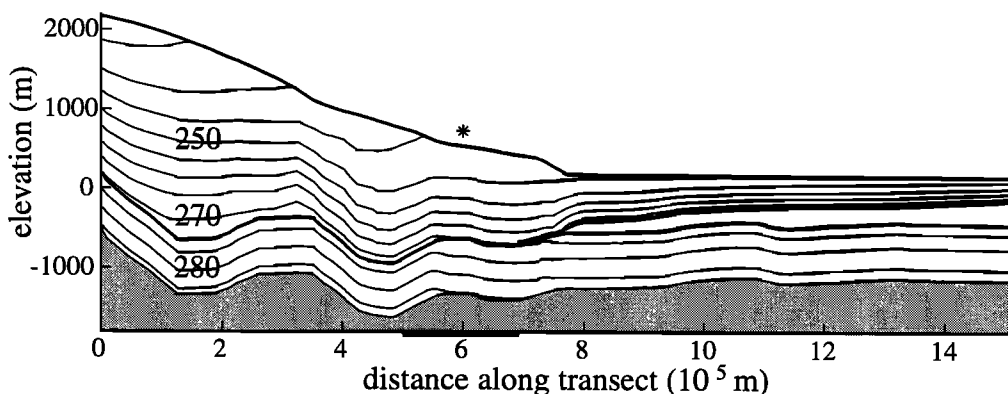


Figure 15. Ice and bedrock temperature at the end of the thermal equilibration with flow law parameters are set at cold ice values, along the cross section that includes Ice Stream B. The contour interval is 5 K. The ice/bed boundary is drawn with a heavy line. The region of ice stream flow is underscored by a heavy line and the location of the UpB camp is denoted by an asterisk.

ice fabric or temperature changes at the ice stream margins. We are now at work implementing a new theory of till mechanics [Tulaczyk, 1998], in which till strength depends on till porosity, to determine basal drag beneath ice streams. Models that simulate the effects of various basal conditions on ice/bed coupling can be used in conjunction with the ice flow model presented here for both investigative and prognostic studies.

The model also demonstrates the well-known incongruity between the downstream increase in ice stream speed and decrease in driving stress (ice thickness). The solution may be found in downstream changes in basal friction or in side drag afforded by the margins. There may be temporal, in addition to spatial, changes in these boundaries. The model developed here, used together with field observations, is a good interpretive tool to study those possibilities and other boundary condition issues.

Notation

Variables used in model equations

- \dot{a} upper surface accumulation rate, positive for accumulation and negative for melting, m/yr.
- A ice flow law rate factor used for inland ice, calculated as $a \exp(-Q/(RT^*))$, $\text{Pa}^{-3} \text{s}^{-1}$.
- \dot{b} lower surface accumulation rate, positive for accumulation (freezing) and negative for melting, m/yr.
- \bar{B} flow law rate factor used for floating ice, calculated as $A^{-1/n}$, $\text{Pa} \text{s}^{-1/3}$.
- E flow law enhancement factor, nondimensional.
- h ice sheet thickness, equal to $z_s - z_b$, m.
- h_{mw} ice sheet basal melt water (fresh water) thickness, m.
- H_i heat flux into the ice from the ice/bed interface, W m^{-2} .
- H_o heat flux in the ice just above the ice/bed interface, W m^{-2} .

- t time, years.
- T temperature, K.
- T_a mean annual surface temperature, K.
- T_{pmp} pressure-dependent melt temperature, calculated as $T_o - \rho g(z_s - z)\Phi$, K.
- $T(z_b)$ basal ice temperature, K.
- T^* homologous temperature, calculated as $T - T_{pmp}$, K.
- \mathbf{u} horizontal velocity vector, m/yr.
- u, v, w velocity component in (x, y, z) direction, respectively, m/yr.
- W viscous heating in ice, W m^{-2} .
- W_b frictional heating at ice/bed interface, W m^{-2} .
- x, y, z axes and locations in Cartesian coordinate system, m.
- z_b ice sheet base elevation, m.
- z_r bedrock surface elevation, m.
- z_s ice sheet surface elevation, m.
- z_{sl} sea surface elevation, m.
- z_+ positive side of the ice/bed interface, m.
- z_- negative side of the ice/bed interface, m.
- β basal flow resistance parameter for ice streams, Pa s/m .
- λ thickness of bedrock layer, m.
- ω temperature oscillation frequency at ice/bed interface, s^{-1} .
- τ_b basal shear stress, Pa.
- ν_e effective viscosity used in flow law for floating ice, Pa s.

Constants used in model equations

- a rate constant factor, 7.23×10^{-12} if $T^* < 263$ K and 3.47×10^4 if $T^* \geq 263$ K, $\text{Pa}^{-3} \text{s}^{-1}$.
- c heat capacity of ice, $2115.3 + 7.79293(T - T_o)$, $\text{J kg}^{-1} \text{K}^{-1}$.
- c_r heat capacity of bedrock, assumed sedimentary, $1000 \text{ J kg}^{-1} \text{K}^{-1}$.
- D_a diffusivity of asthenosphere, $1 \times 10^8 \text{ m}^2/\text{yr}$.
- g acceleration due to gravity, 9.81 m s^{-2} .

G	geothermal heat flux, 0.0669 W m^{-2} .
k	thermal conductivity of ice, $3.101 \times 10^8 \exp(-0.0057T)$, W m K^{-1} .
k_r	thermal conductivity of bedrock (sedimentary), 3.3 W m K^{-1} .
L_f	latent heat of fusion for water, $3.35 \times 10^5 \text{ J/kg}$.
n	exponent in Glen's flow law for ice, 3.
Q	activation energy for creep flow of ice, 6.0×10^4 if $T^* < 263 \text{ K}$ and 13.9×10^4 if $T^* \geq 263 \text{ K}$, J/mol .
R	gas constant, 8.31 J/mol/K .
T_o	triple point of water, 273.15 K .
Φ	dependence of melting temperature on pressure, $8.71 \times 10^{-4} \text{ K/Pa}$.
ρ	density of ice, 910 kg m^{-3} .
ρ_a	density of asthenosphere, 3000 kg m^{-3} .
ρ_r	density of bedrock (sedimentary), 2700 kg m^{-3} .
ρ_w	density of seawater at melt temperature, 1027 kg m^{-3} .

Acknowledgments. This work was supported by a NASA Graduate Student Fellowship in Global Change Research (to C. L. Hulbe) and NSF grant ATM-9870875. B. Parizek, C. S. Jackson, and J. A. van Zanten were indispensable for intellectual and computational contributions. The comments of an anonymous reviewer and R. Kwok helped finish this rather long contribution.

References

- Alley, R. B., and I. M. Whillans, Changes in the West Antarctic Ice Sheet, *Science*, 254, 959-963, 1991.
- Barclon, V., and D.R. MacAyeal, Steady flow of a viscous ice stream across a no-slip/slip-free transition at the bed, *J. Glaciol.*, 39(131), 167-185, 1993.
- Bell, R.E., D.D. Blankenship, C.A. Finn, D.L. Morse, T.A. Scambos, J.M. Brozena, and S.M. Hodge, Influence of subglacial geology on the onset of a West Antarctic ice stream from aerogeophysical observations, *Nature*, 394, 58-62, 1998.
- Bromwich, D.H., Precipitation regime of the West Antarctic Ice Sheet, in *Environment of West Antarctica: Potential CO₂-Induced Changes*, pp. 107-115, Nat. Acad. Press, Washington, D.C., 1984.
- Budd, W.F., B.J. McInnes, D. Jansen, and I.N. Smith, Modelling the response of the West Antarctic Ice Sheet to a climatic warming, in *Dynamics of the West Antarctic Ice Sheet*, edited by C.J. van der Veen and J. Oerlemans, pp. 321-358, D. Reidel, Norwell, Mass., 1987.
- Carlsaw, H.S., and J.C. Jaeger, *Conduction of Heat in Solids*, 510 pp, Clarendon, Oxford, England, U.K., 1988.
- Chen, X., R.A. Bindschadler, and P.L. Vornberger, Determination of velocity field and strain rate field in West Antarctica using high-precision GPS measurements, *Surv. and Land Inf. Syst.*, 58(4), 247-255, 1998.
- Drewry, D.J. (Ed.), *Antarctic Glaciological and Geophysical Folio*, Scot Polar Res. Inst., Cambridge, England, U.K., 1983.
- Echelmeyer, K.A., W.D. Harrison, C. Larsen, and J.E. Mitchell, The role of the margins in the dynamics of an active ice stream, *J. Glaciol.*, 40(136), 527-538, 1994.
- Engelhardt, H. and B. Kamb, Basal hydraulic system of a West Antarctic ice stream: Constraints from borehole observations, *J. Glaciol.*, 43(144), 207-230, 1997.
- Fastook, J.L., Use of a new finite element continuity model to study the transient behavior of ice stream C and causes of its present low velocity, *J. Geophys. Res.*, 92, 8941-8949, 1987.
- Fastook, J.L., and M. Prentice, A finite-element model of Antarctica: Sensitivity test for meteorological mass-balance relationship, *J. Glaciol.*, 40(134), 167-175, 1994.
- Giovinetto, M.B., N.M. Waters, and C.R. Bentley, Dependence of Antarctic surface mass balance on temperature, elevation, and distance to the open ocean, *J. Geophys. Res.*, 95, 3517-3531, 1990.
- Gow, A.J., H.T. Ueda, and D.E. Garfield, Antarctic ice sheet: preliminary results of first core hole to bedrock, *Science*, 161, 1011-1013, 1968.
- Greve, R., Thermomechanisches Verhalten polythermer Eisschilde Theorie, Analytik, Numerik, Ph.D. thesis, Tech. Hochsch., Darmstadt, Germany, 1995.
- Hindmarsh, R.C.A., Modelling the dynamics of ice sheets, *Prog. Phys. Geogr.*, 17(4), 391-412, 1993.
- Hooke, R. L., Flow law for polycrystalline ice in glaciers: Comparison of theoretical predictions, laboratory data, and field measurements, *Rev. Geophys.*, 19(4), 664-672, 1981.
- Hulbe, C.L., An ice shelf mechanism for Heinrich layer production, *Paleoceanography*, 12(5), 711-717, 1997.
- Hulbe, C.L., Heat balance of West Antarctic ice streams, investigated with a numerical model of coupled ice sheet, ice stream, and ice shelf flow, Ph.D. thesis, Univ. of Chicago, Chicago, Ill., 1998.
- Hutter, K., *Theoretical Glaciology*, D. Reidel, Norwell, Mass., 1983.
- Huybrechts, P., A three-dimensional numerical model for the Antarctic ice sheet: A sensitivity study on the glacial-interglacial contrast, *Clim. Dyn.*, 5, 79-92, 1990.
- Huybrechts, P., and J. Oerlemans, Evolution of the East Antarctic Ice Sheet: A numerical study of thermomechanical response patterns with changing climate, *Ann. Glaciol.*, 11, 52-59, 1988.
- Huybrechts, P., and J. Oerlemans, Response of the Antarctic ice sheet to future greenhouse warming, *Clim. Dyn.*, 5, 93-102, 1990.
- Jackson, M., and B. Kamb, The marginal shear stress of Ice Stream B, West Antarctica, *J. Glaciol.*, 43(145), 415-426, 1997.
- MacAyeal, D.R., Transient temperature-depth profiles of the Ross Ice Shelf, M.S. thesis, Univ. of Maine, Orono, Maine, 1979.
- MacAyeal, D.R., Large-scale ice flow over a viscous basal sediment: Theory and application to Ice Stream B, Antarctica, *J. Geophys. Res.*, 94, 4071-4087, 1989.
- MacAyeal, D.R., and R.H. Thomas, Numerical modeling of ice shelf motion, *Ann. Glaciol.*, 3, 189-193, 1982.
- MacAyeal, D.R., R.A. Bindschadler, and T.A. Scambos, Basal friction of Ice Stream E, West Antarctica, *J. Glaciol.*, 41(138), 247-262, 1995.
- MacAyeal, D.R., V. Rommelaere, P. Huybrechts, C.L. Hulbe, J. Determann, and C. Ritz, An ice shelf model test based on the Ross Ice Shelf, *Ann. Glaciol.*, 23, 46-51, 1996.
- Oerlemans, J., and C.J. van der Veen, *Ice Sheets and Climate*, 217 pp., D. Reidel, Norwell, Mass., 1984.
- Paterson, W.S.B., *The Physics of Glaciers*, 2nd ed., 380 pp, Pergamon, Tarrytown, N.Y., 1981.
- Payne, A. J., Limit cycles in the basal thermal regime of ice sheets, *J. Geophys. Res.*, 100, 4249-4263, 1995.
- Payne, A.J., and P.W. Dongelmans, Self-organization in the thermomechanical flow of ice sheets, *J. Geophys. Res.*, 102, 12219-12234, 1997.
- Raymond, C.F., Shear margins in glaciers and ice sheets, *J. Glaciol.*, 40(142), 90-102, 1996.

- Robin, G. de Q., General glaciology, in *The Climatic Record in Polar Ice Sheets*, edited by G. de Q. Robin, pp. 94-97, Cambridge University Press, New York, 1983.
- Shabtaie, S., I.M. Whillans, and C.R. Bentley, The morphology of ice streams A, B, and C, West Antarctica, and their environs, *J. Geophys. Res.*, *92*, 8865-8883, 1987.
- Tulaczyk, S.M., Basal mechanics and geologic record of ice streaming, West Antarctica, Ph.D. thesis, Calif. Inst. of Technol., Pasadena, 1998.
- Vaughan, D.G., J.L. Bamber, M. Giovinetto, J. Russell, and A.P.R. Cooper, Reassessment of net surface mass balance in Antarctica, *J. Clim.*, *12*(4), 933-946, 1999.
- Whillans, I.M., The equation of continuity and its application to the ice sheet near "Byrd" Station, Antarctica, *J. Glaciol.*, *18*(80), 359-371, 1977.
- Whillans, I.M., and C.J. van der Veen, Patterns of calculated basal drag on Ice Streams B and C, Antarctica, *J. Glaciol.*, *39*(133), 437-446, 1993a.
- Whillans, I.M., and C.J. van der Veen, New and improved determinations of velocity of Ice Streams B and C, West Antarctica, *J. Glaciol.*, *39*(133), 483-490, 1993b.
- Whillans, I.M., and C.J. van der Veen, The role of lateral drag in the dynamics of Ice Stream B, Antarctica, *J. Glaciol.*, *43*(144), 231-237, 1997.
- Whillans, I.M., M. Jackson, and Y-H. Tseng, Velocity pattern in a transect across Ice Stream B, Antarctica, *J. Glaciol.*, *39*(133), 562-572, 1993.

C. L. Hulbe, NASA Goddard Space Flight Center, Code 971, Greenbelt, MD 20771. (chulbe@ice.gsfc.nasa.gov)

D. R. MacAyeal, Department of Geophysical Sciences, University of Chicago, 5807 S. Ellis Ave., Chicago, IL 60637. (drm7@midway.uchicago.edu)

(Received March 2, 1999; revised July 13, 1999; accepted July 23, 1999.)